Electronic Supplementary Material (ESI) for Dalton Transactions.
This journal is © The Royal Society of Chemistry 2022

Supporting Information

Ru- and Ir-complexes decorated periodic mesoporous organosilicas as sensitizers for artificial photosynthesis

Raúl Rojas-Luna,[a] Miguel Castillo-Rodríguez,[b] José R. Ruiz,[a] César Jiménez-Sanchidrián,[a] Dolores Esquivel[a*] and Francisco J. Romero-Salguero[a*]

[a]Departamento de Química Orgánica, Instituto Químico para la Energía y el Medioambiente (IQUEMA), Facultad de Ciencias, Universidad de Córdoba, Campus de Rabanales, 14071 Córdoba, Spain.

[b]Departamento de Física Aplicada, Radiología y Medicina Física, Universidad de Córdoba, Campus de Rabanales, 14071 Córdoba, Spain

* q12esmem@uco.es (D.E.); qo2rosaf@uco.es (F.J.R.-S.)

Table S1. Comparison of Ndppz-PMO with previously reported materials functionalized through Diels-Alder reaction with 3,6-di-(2-pyridyl)-1,2,4,5-tetrazine.

Materials	**DA-conditions**		**N-loading (%)**	**N-loading (mmol N/g)**	**Ref.**
	T[a] (ºC)	**time (days)**			
dppz-ePMO	200	11 days[a]	1.00	0.18	[1,2]
dppz-vSilica	200	11 days[a]	0.65	0.12	[2,3]
dppz-vPMO	150	11 days[b]	1.00	0.18	[4]
Ndppz-PMO	RT[c]	30 min[c]	2.03	0.36-0.39	This work

[a] reaction mixture aged in an autoclave
[b] reaction mixture refluxed in dodecane
[c] reaction mixture for the synthesis of Ndppz precursor in anhydrous THF. It was subsequent used in the synthesis of Ndppz-PMO material

1 D. Esquivel, A. M. Kaczmarek, C. Jiménez-Sanchidrián, R. Van Deun, F. J. Romero-Salguero and P. Van der Voort, *J. Mater. Chem. C*, 2015, **3**, 2909–2917.

2 A. M. Kaczmarek, D. Esquivel, J. Ouwehand, P. Van Der Voort, F. J. Romero-Salguero and R. Van Deun, *Dalt. Trans.*, 2017, **46**, 7878–7887.

3 A. M. Kaczmarek, D. Esquivel, B. Laforce, L. Vincze, P. Van Der Voort, F. J. Romero-Salguero and R. Van Deun, *Luminescence*, 2018, **33**, 567–573.

4 M. Á. Navarro, J. Amaro-Gahete, J. R. Ruiz, C. Jiménez-Sanchidrián, F. J. Romero-Salguero and D. Esquivel, *Dalt. Trans.*, 2022, **51**, 4884–4897.

Experimental Section

Chemicals and materials. Reagents and solvents were obtained from commercial sources and used as received without further purification. Hydrazine hydrate (50-60%), 2-pyridinecarbonitrile (99%) and sodium nitrite (97%) were purchased from Aldrich for the synthesis of 3,6-di-2-pyridyl-1,2,4,5-tetrazine. 5-Norbornen-2-yltriethoxysilane, also named 5-(bicycloheptenyl)triethoxysilane (97%, Fluorochem), 2,3-dichloro-5,6-dicyano-*p*-benzoquinone (DDQ, 98%, Aldrich) and anhydrous tetrahydrofuran (Aldrich) were used for the synthesis of the organosilane precursor (Ndppz). 1,2-Bis(triethoxysilyl)ethane (BTEE, 97%, abcr), octadecyltrimethylammonium bromide (OTAB, 98%, Aldrich), sodium hydroxide (99%, Aldrich) and ethanol (Absolute, Labkem) were employed for the synthesis of NdppzPMO material. Cis-dichlorobis(2,2′-bipyridine)ruthenium(II) hydrate (97%, Aldrich), dichlorotetrakis(2-(2-pyridinyl)phenyl)diiridium(III) (100%, Aldrich) and potassium hexachloroplatinate(IV) (98%, Aldrich) were utilized for the preparation of the Ru- and Ir- complexes and the subsequent deposition of the platinum precursor on the pore surface. Methyl viologen dichloride hydrate (MV, 98%, Aldrich), ethylenediamine tetraacetic acid (EDTA, 99%, Aldrich) and acetate buffer solution (1 M, pH= 5.0) were used in the photocatalytic reactions for hydrogen production.

Characterization. ^{1}H and ^{13}C NMR spectrum were recorded on a Bruker spectrometer at 300 MHz with $CDCl_3$ as solvent. Powder X-ray diffraction patterns were performed on a Bruker D8 Discover A25 diffractometer using Cu Kα radiation (40 kV and 30 mA) from 0.5 to 5.0 (2θ). N_2 adsorption-desorption isotherms were collected using an Autosorb-iQ MP/-XR instrument. Prior to the measurement, samples were outgassed at 120 ºC overnight. The Brunauer-Emmett-Teller (BET) method was used to estimate surface areas while pore diameter and pore volume were estimated using Density Functional Theory (DFT) with a specific DFT model (N_2 at 77 K on silica, cylindrical pore, NLDFT equilibrium model). Microstructural analysis was accomplished by TEM using a FEI Talos F200X S/TEM microscope operating at 200 kV. Both conventional TEM and STEM mode using high angle annular dark field (HAADF) imaging were performed. Elemental mapping was carried out using energy dispersive X-ray spectroscopy (EDS). The solid-state ^{13}C CP/MAS NMR measurements were performed on a Bruker Avance III HD 400 WB spectrometer at 13 kHz. The excitation pulse and recycle time for NMR measurements were 3.6 ms and 2 s, respectively. Chemical shifts were referenced to

tetramethylsilane (TMS) standard. Raman spectrum of the samples were acquired with a Renishaw Raman spectrometer. X-ray photoelectron spectroscopy (XPS) were recorded on a SPECS Phoibos HAS 3500 150 MCD X-ray photoelectron spectrometer with a monochromatic Al X-ray source (1486.7 eV). Binding energies (BE) were determined with respect to the position of the Si 2p peak at 103.4 eV. The charge neutralization function was used to compensate for accumulated charge in solid samples by X-ray irradiation. UV-Vis diffuse reflectance measurements were acquired on a Perkin Elmer Lambda 650 S UV/Vis spectrometer using a 150 mm integrating sphere and operating in a double beam mode. Elemental analysis (CHN) was performed on a LECO TRUSPEC CHNS MICRO elemental analyzer. Inductively coupled plasma mass spectrometry (ICP-MS) for isotopes ^{101}Ru, ^{192}Ir and ^{195}Pt were measured using a Perkin Elmer NexION 350X spectrometer. Prior to the measurement, the sample was digested in an UltraWave microwave system.

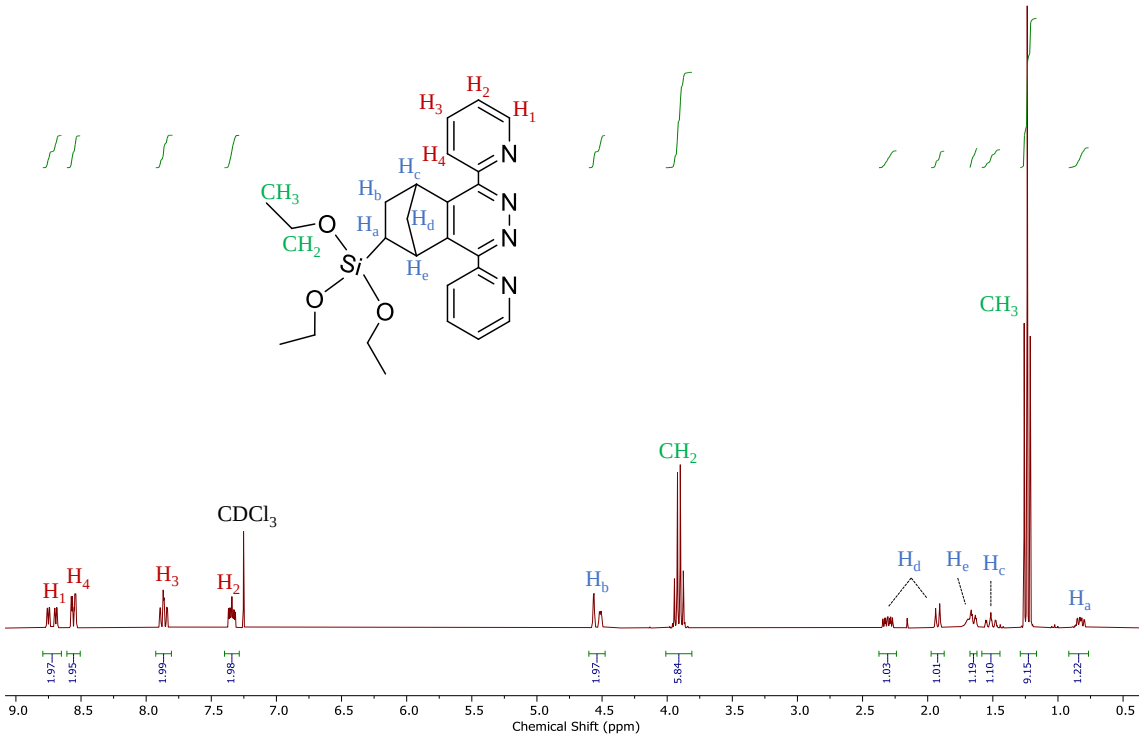

Fig. S1. ^{1}H NMR spectrum of Ndppz precursor in $CDCl_3$.

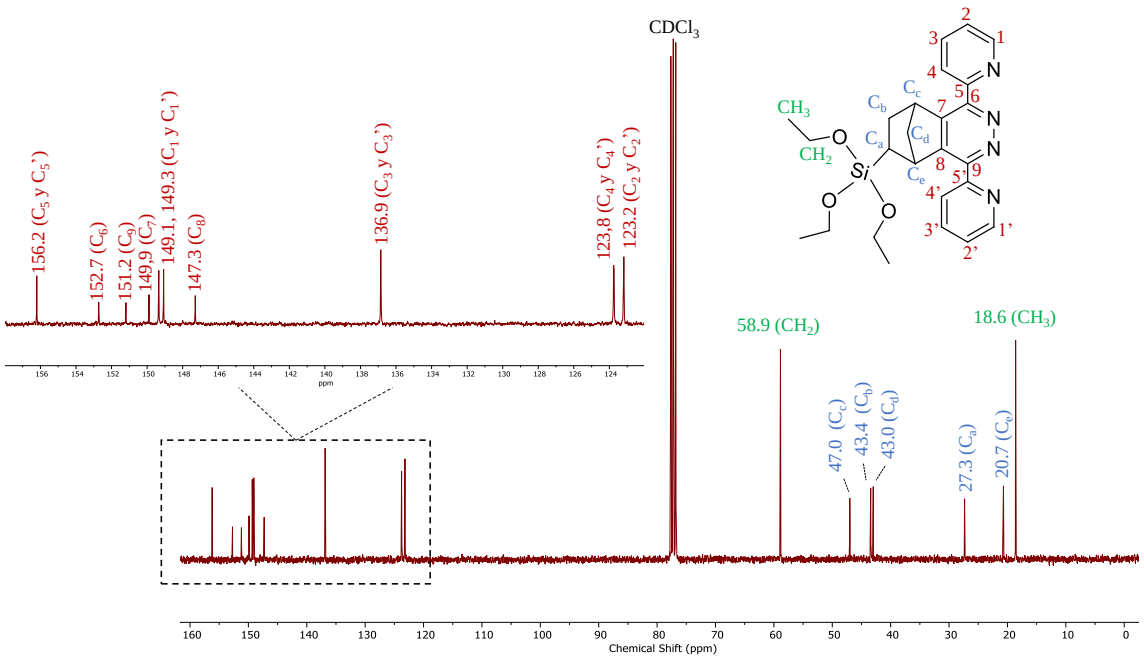

Fig. S2. ^{13}C NMR spectrum of Ndppz precursor in $CDCl_3$.

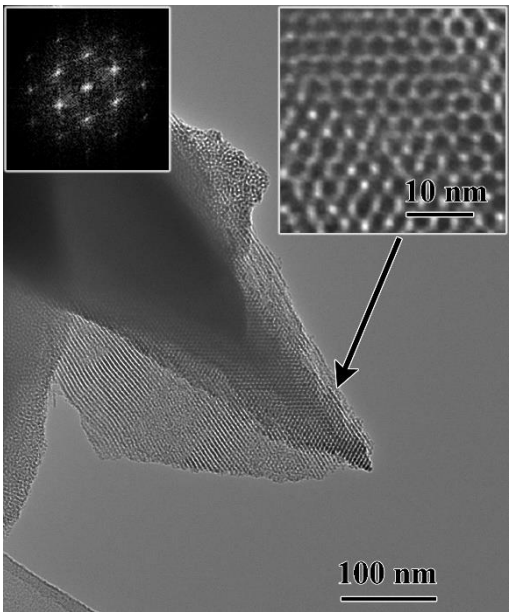

Fig. S3. TEM image of NdppzPMO. The upper right inset shows the arrangement of pores whose FFT diagram (upper left inset) indicates a highly ordered hexagonal mesostructure.

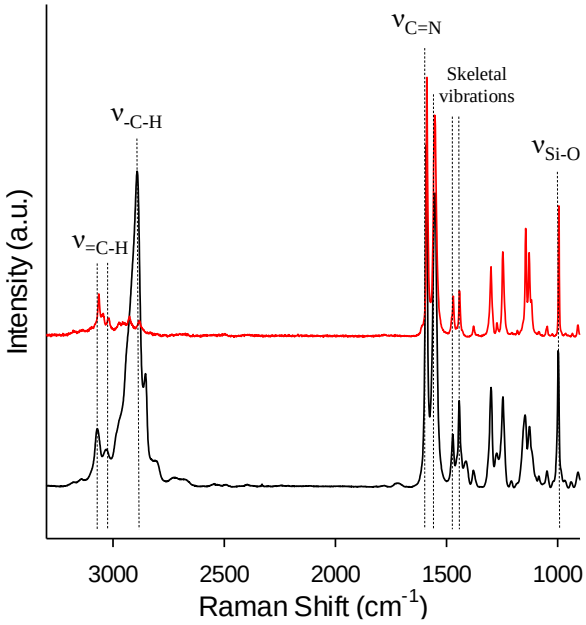

Fig. S4. Raman spectrum of Ndppz precursor (red solid line) and NdppzPMO (black solid line).

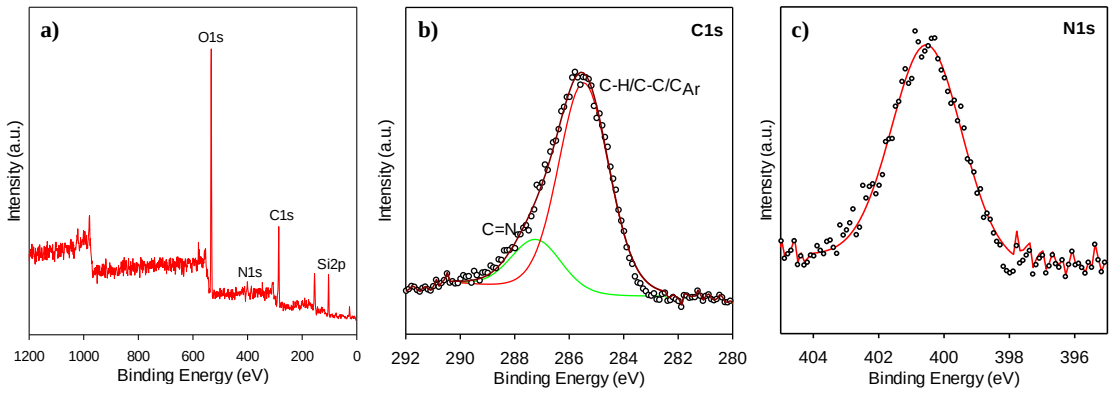

Fig. S5. XPS spectrum of NdppzPMO: (a) survey scan, (b) C1s and (c) N1s.

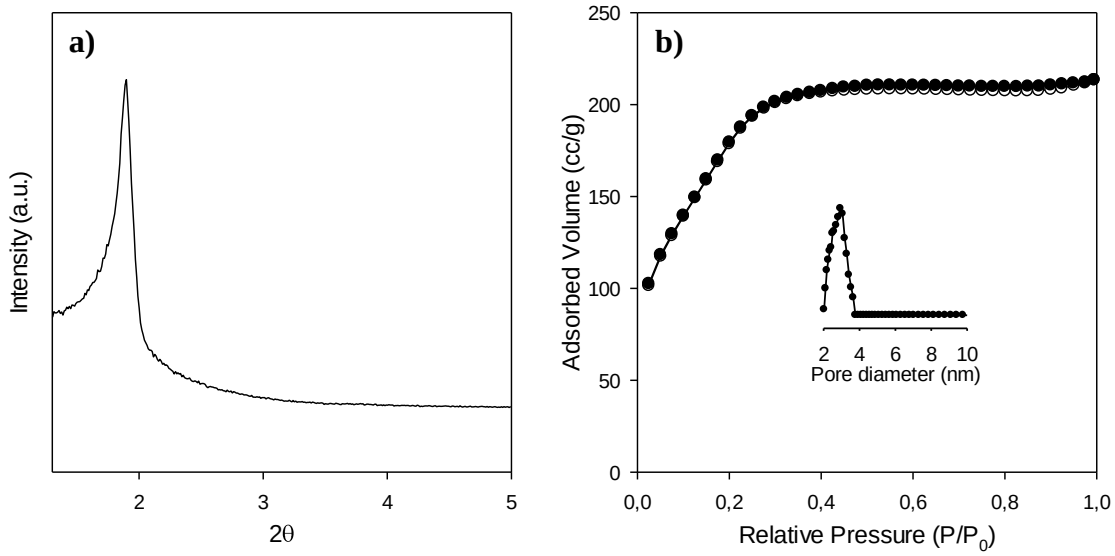

Fig. S6. (a) X-ray diffraction pattern and (b) N_2 adsorption/desorption isotherms and pore size distribution (inset) of Ru@NdppzPMO.

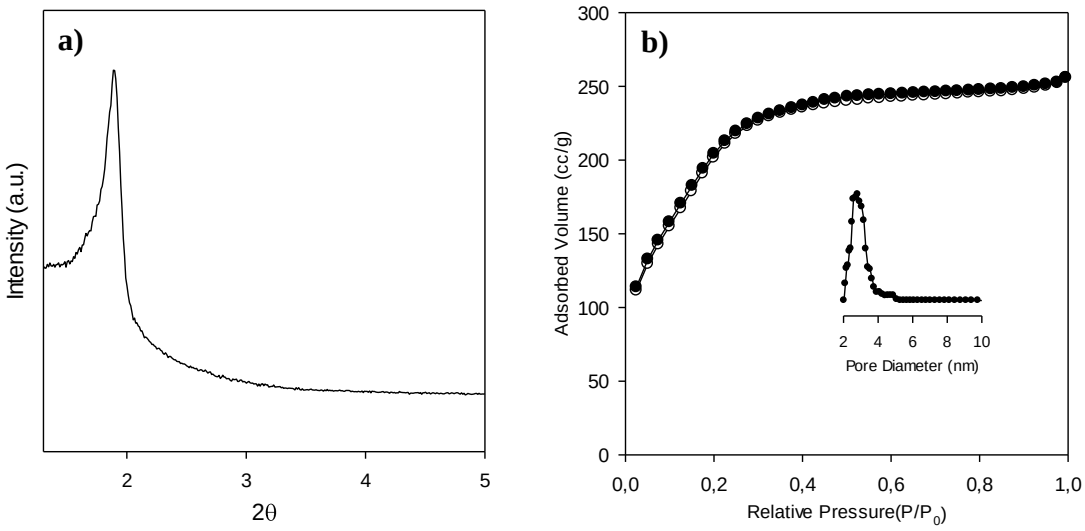

Fig. S7. (a) X-ray diffraction pattern and (b) N_2 adsorption/desorption isotherms and pore size distribution (inset) of Ir@NdppzPMO.

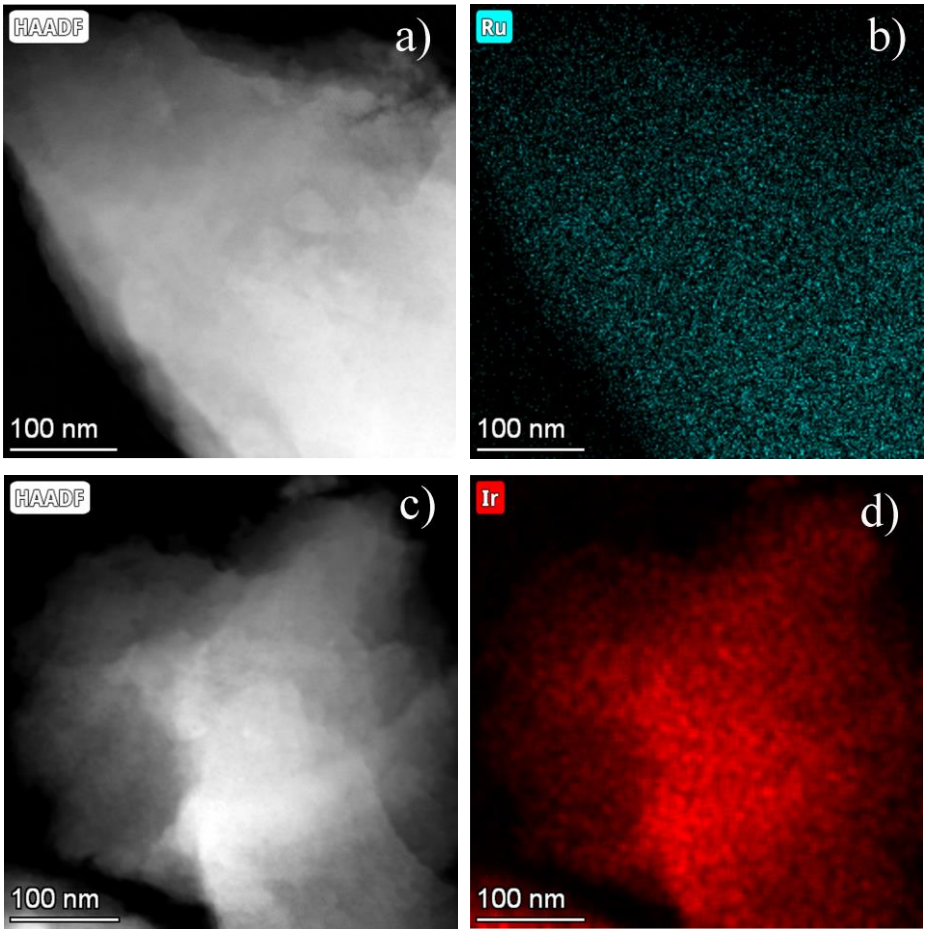

Fig. S8. HAADF-STEM image for (a) Ru@NdppzPMO and (c) Ir@NdppzPMO samples. EDS elemental mapping for (b) Ru and (d) Ir are also shown.

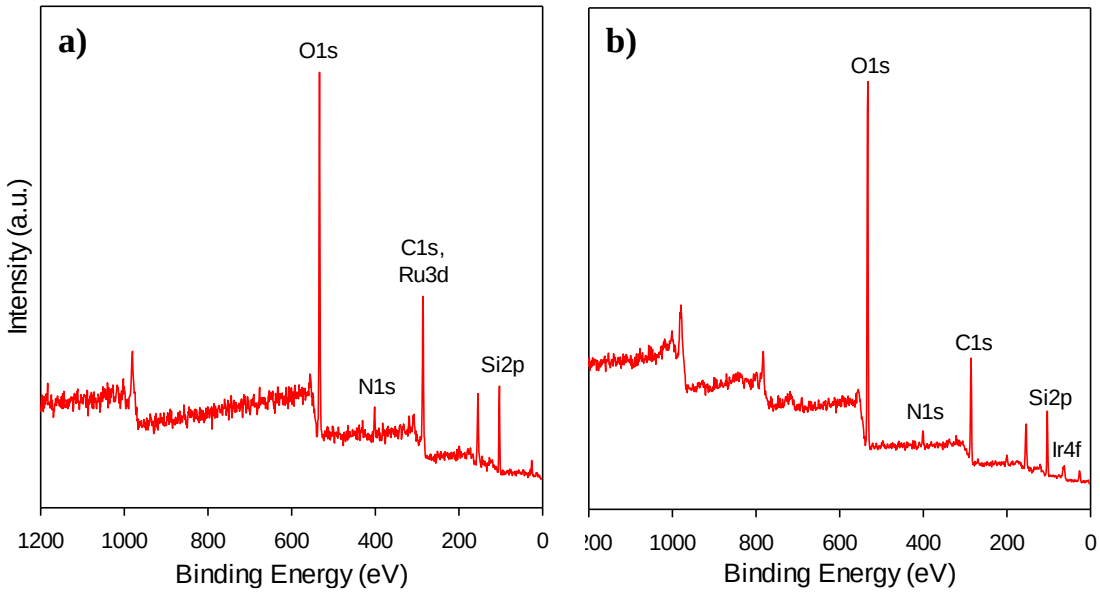

Fig. S9. XPS survey spectrum: a) Ru@NdppzPMO and (b) Ir@NdppzPMO

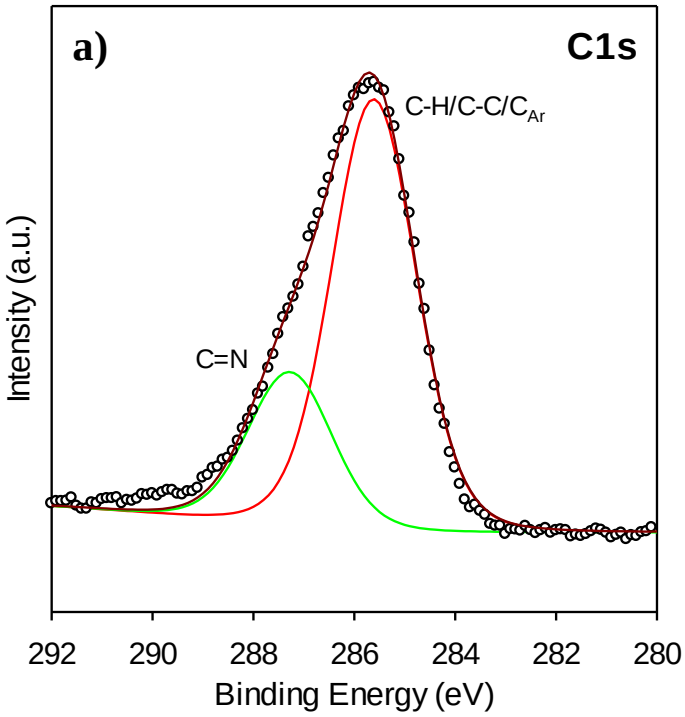

Fig. S10. C1s XPS spectrum of Ir@NdppzPMO.

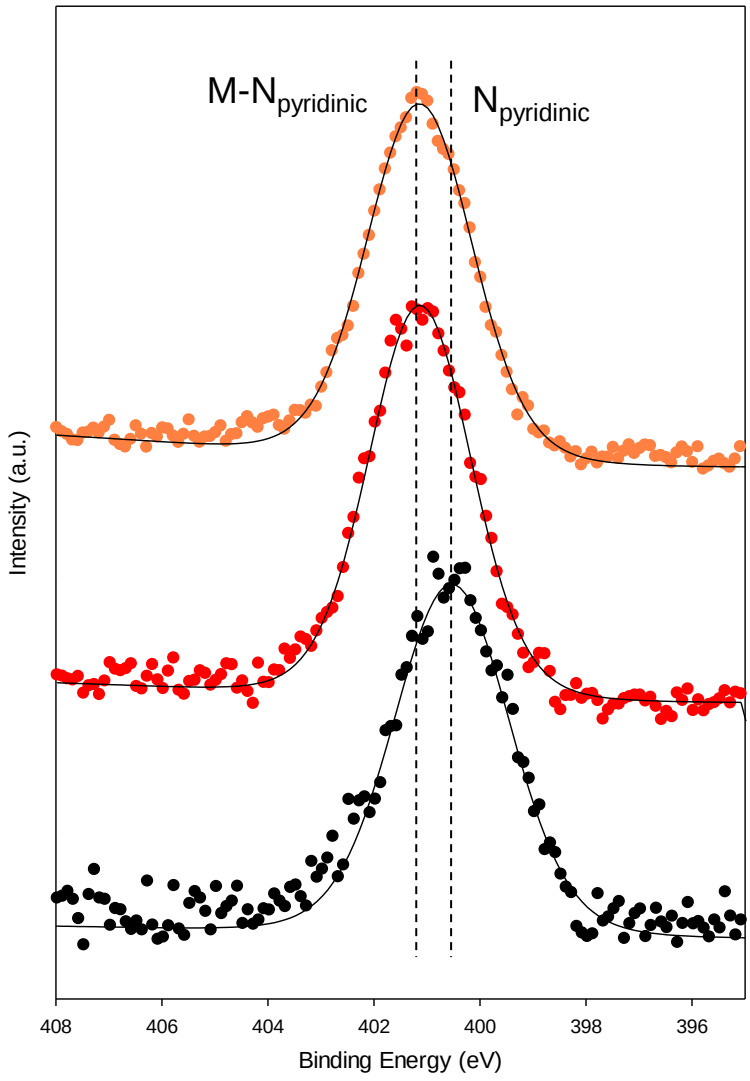

Fig. S11. N1s core level XPS spectrum of NdppzPMO (black), Ru@NdppzPMO (red) and Ir@NdppzPMO (orange).

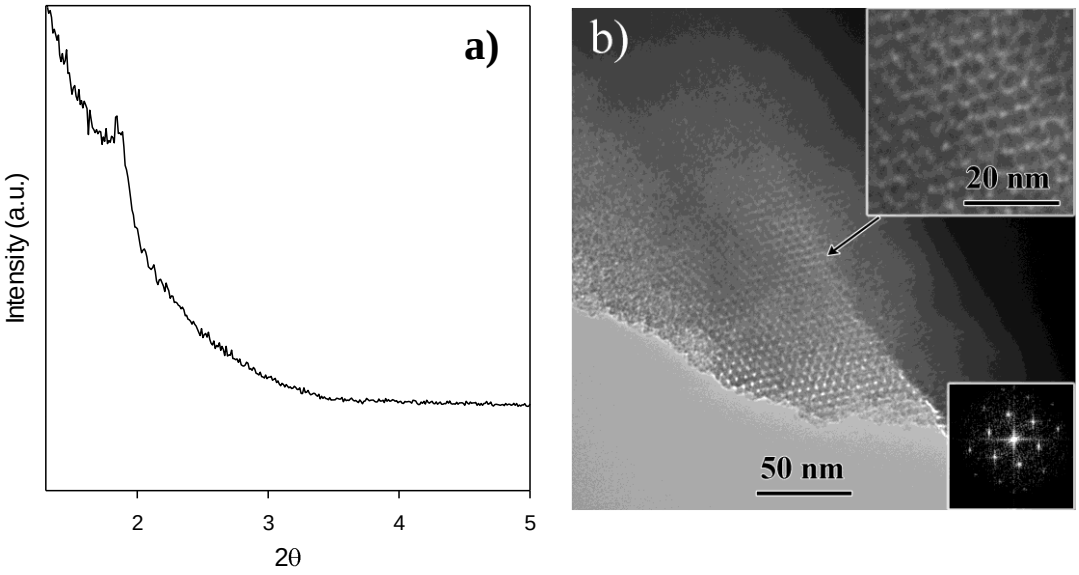

Fig. S12. (a) X-ray diffraction pattern of Pt/Ru@NdppzPMO and (b) TEM image of Pt/Ru@NdppzPMO. Insets at higher magnification and the FFT pattern evidence the preservation of the highly ordered hexagonal mesostructure.

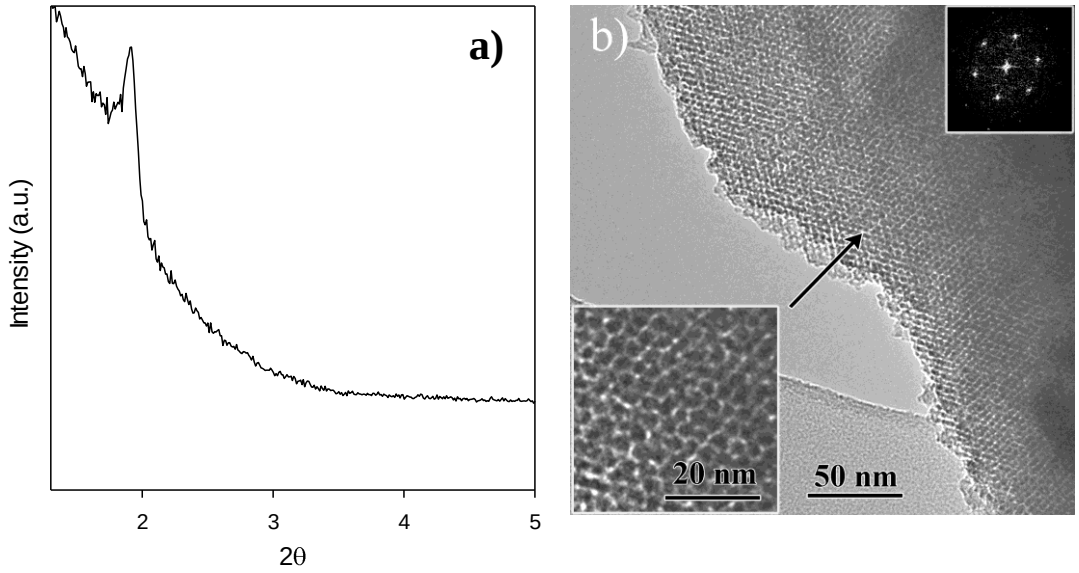

Fig. S13. (a) X-ray diffraction pattern Pt/Ir@NdppzPMO and (b) TEM image of Pt/Ir@NdppzPMO. Insets at higher magnification and the FFT pattern evidence the preservation of the highly ordered hexagonal mesostructure.

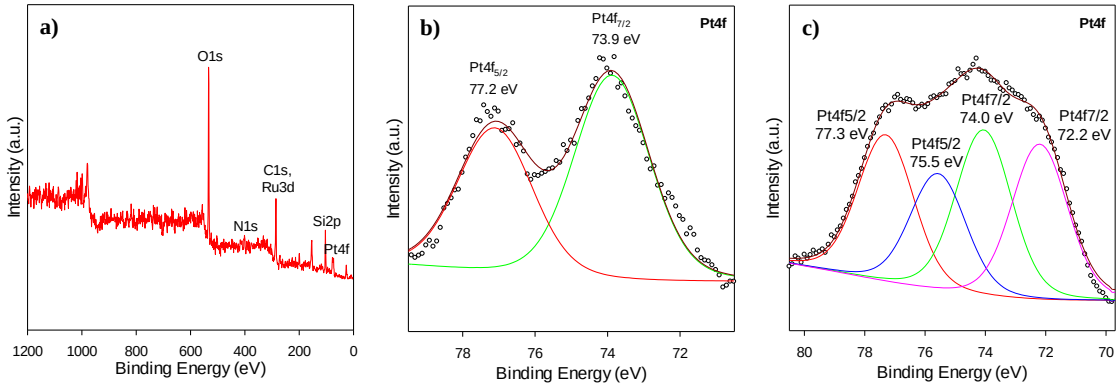

Fig. S14. XPS spectrum of Pt/Ru@NdppzPMO: (a) Survey scan, (b) Pt4f before irradiation with visible light and (c) Pt4f after 24 h of irradiation with visible light.

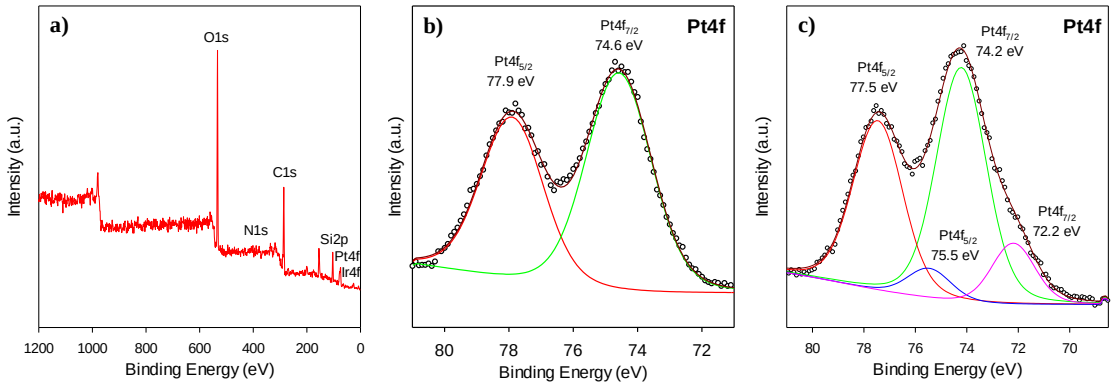

Fig. S15. XPS spectrum of Pt/Ir@NdppzPMO: (a) Survey scan, (b) Pt4f before irradiation with visible light and (c) Pt4f after 24 h of irradiation with visible light.

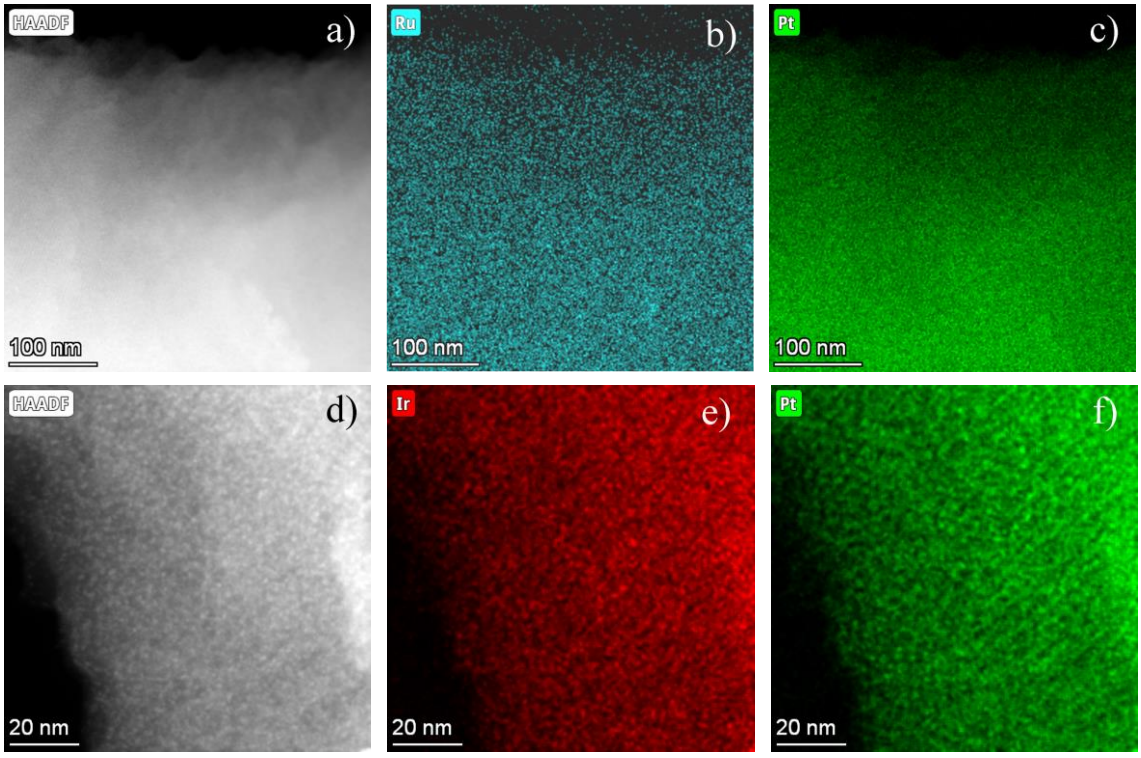

Fig. S16. (a) HAADF-STEM image, (b) Ru and (c) Pt elemental mappings for Pt/Ru@NdppzPMO sample. (d), (e) and (f) correspond to HAADF-STEM, Ir and Pt elemental mapping for Pt/Ir@NdppzPMO sample, respectively.

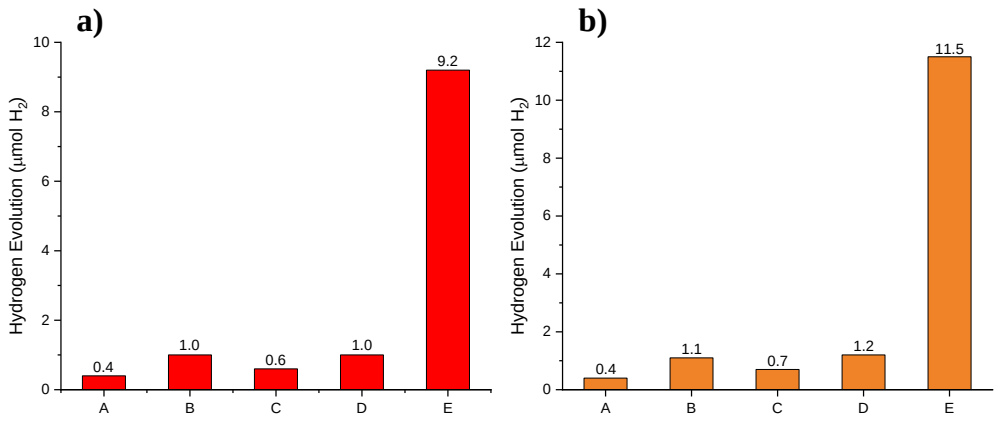

Fig. S17. Control reactions for Ru@NdppzPMO (a) and Ir@NdppzPMO (b) systems. Reaction conditions: using ethylene-bridged PMO without photosensitizer unit (A), absence of catalyst (B), using M@NdppzPMO (PS) and K_2PtCl_6 (Cat) in absence of MV (ER) (C) using Pt/M@NdppzPMO (PS and Cat) in absence of MV (ER) (D), three-component HER (E).

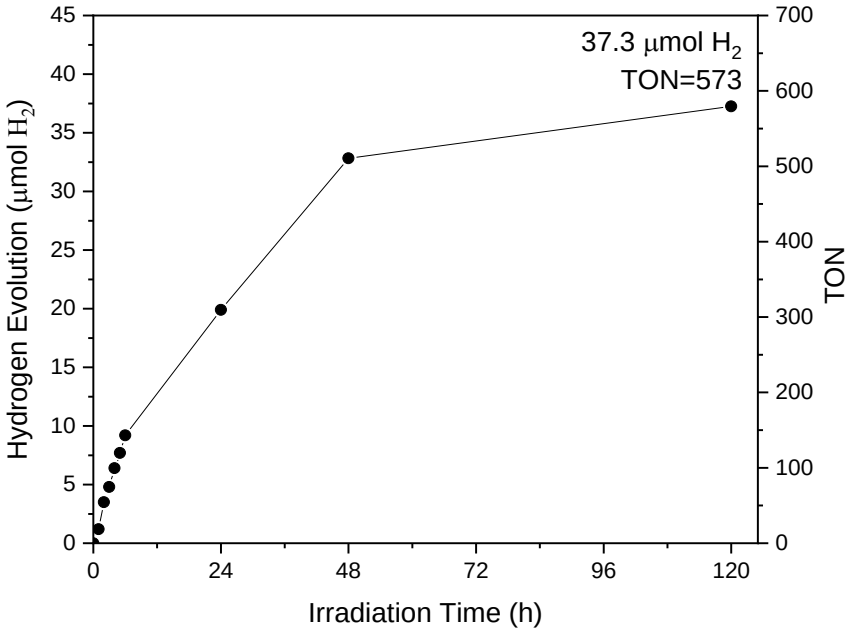

Fig. S18. Time course for photocatalytic hydrogen production by Pt/Ru@NdppzPMO for 120 h of reaction.

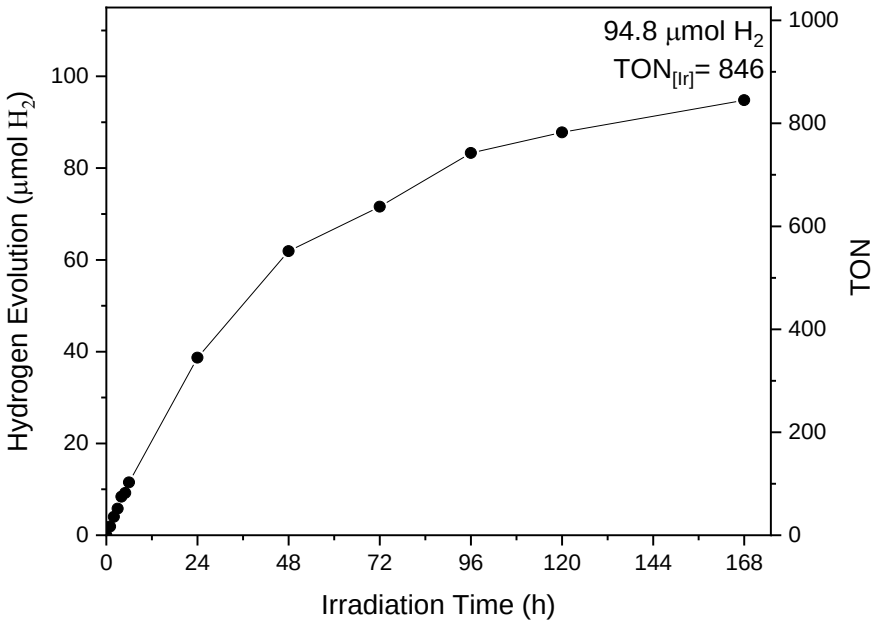

Fig. S19. Time course for photocatalytic hydrogen production by Pt/Ir@NdppzPMO for 168 h of reaction.

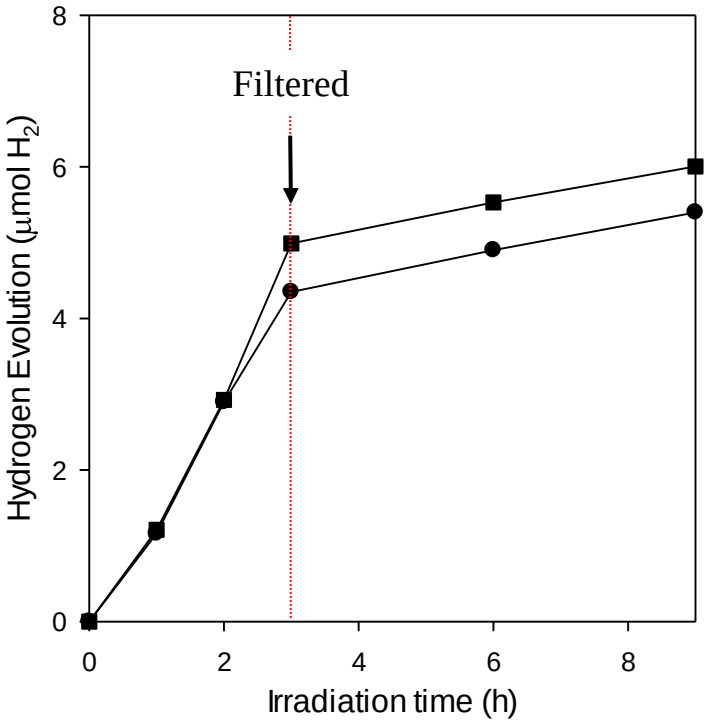

Fig. S20. Filtration experiments for Pt/Ru@NdppzPMO (circle) and Pt/Ir@NdppzPMO (square).

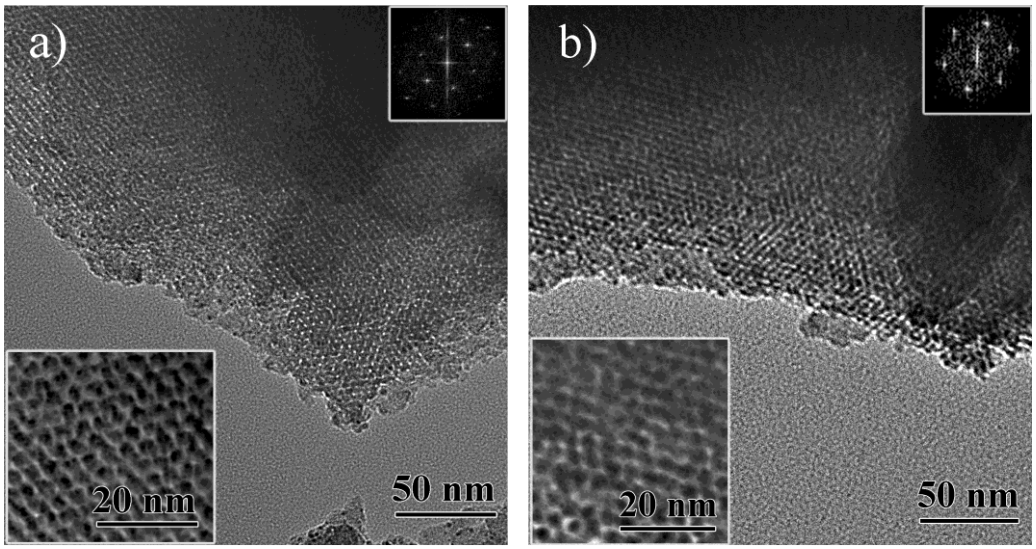

Fig. S21. Conventional TEM images for (a) Pt/Ru@NdppzPMO and (b) Pt/Ir@NdppzPMO both after 24 h of irradiation. Higher magnification and FFT pattern insets confirm the stability of the ordered mesostructures.

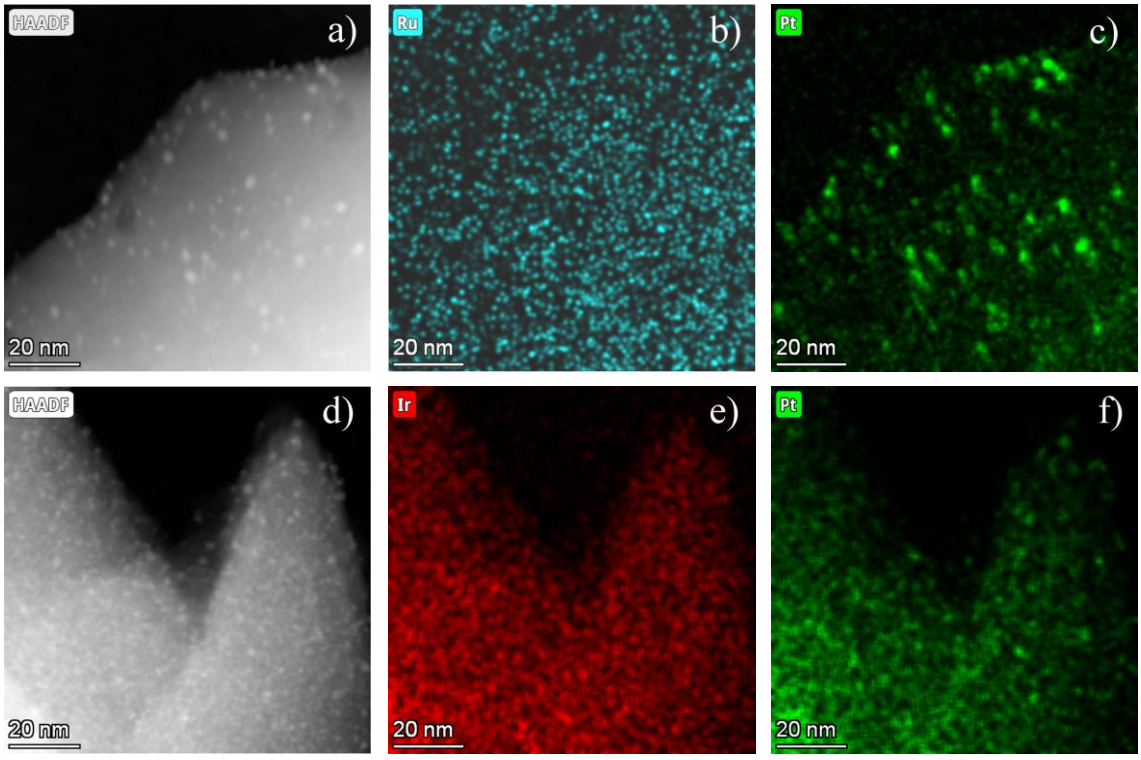

Fig. S22. HAADF-STEM images for (a) Pt/Ru@NdppzPMO and (d) Pt/Ir@NdppzPMO both after 24 h of irradiation. Ru, Ir and Pt EDS maps are accompanying HAADF-STEM images.